Journal of Theoretical Biology 525 (2021) 110749

Contents lists available at ScienceDirect

Journal of Theoretical Biology

journal homepage: www.elsevier.com/locate/yjtbi

The role of syncytia during viral infections

Benjamin Jessie, Hana M. Dobrovolny *

Department of Physics and Astronomy, Texas Christian University, Fort Worth, TX, United States

ARTICLE INFO

Article history:
Received 12 October 2020
Revised 25 March 2021
Accepted 29 April 2021
Available online 05 May 2021

Keywords:
Respiratory syncytial virus
Viral production
Infectious lifespan
Syncytia formation
Mathematical model

ABSTRACT

Respiratory syncytial virus (RSV) is a common, contagious infection of the lungs and the respiratory tract. RSV is characterized by syncytia, which are multinuclear cells created by cells that have fused together. We use a mathematical model to study how different assumptions about the viral production and lifespan of syncytia change the resulting infection time course. We find that the effect of syncytia on viral titer is only apparent when the basic reproduction number for infection via syncytia formation is similar to the reproduction number for cell free viral transmission. When syncytia fusion rate is high, we find the presence of syncytia can lead to slowly growing infections if viral production is suppressed in syncytia. Our model provides insight into how the presence of syncytia can affect the time course of a viral infection.

1. Introduction

Respiratory syncytial virus (RSV) is a common virus that causes infected lung and respiratory tract cells to fuse together resulting in multinucleated cells called syncytia (Saleh et al., 2020; Domachowske et al., 2000). It is so common it is estimated that most people have had the infection by the age of two (Toivonen et al., 2020). RSV can be continually contracted throughout a person's lifetime with minimal, often no symptoms (Walsh et al., 2004; Ali et al., 2020; Tin Tin Htar et al., 2020). However, those with weakened immune systems, infants, and the elderly could potentially suffer more severe symptoms (Drews et al., 2019; Walsh et al., 2013).

On a cellular level, the infection process begins when a single virus fuses into the cytoplasm of a healthy cell (Bem et al., 2011). Once inside, the virus begins replicating, and the now infected cell releases newly replicated viruses to nearby healthy cells (Piva et al., 2020). The infected cell can continue to produce more virus or fuse with other cells via the fusion protein (Hu et al., 2020; Gonzalez-Reyes et al., 2001; Porotto et al., 2019). While some physical characteristics of syncytia, such as size or number of fused cells (Gagliardi et al., 2017; Ayala-Breton et al., 2014), can easily be measured, some characteristics that affect the infection dynamics are harder to measure directly. For example, if syncytia do not produce as much virus as the individual cells, an infection will be less severe (less overall virus) if there are a large number of syncytia. Or if multinucleated cells enhance production of the virus, the infection will be more severe. Similarly, if the lifespan of syncytia differs from the lifespan of mononucleated cells, we might see an overall lengthening or shortening of the infection as the number of syncytia varies. Without the ability to measure these syncytia characteristics, it is difficult to understand the role of syncytia in the viral infection (Taylor, 2017).

Mathematical models can be used to help elucidate the role syncytia play in the infection. While mathematical modeling has been applied to the study of RSV infections (González-Parra and Dobrovolny, 2015, 2018a; González-Parra et al., 2018; González-Parra and Dobrovolny, 2018b; González-Parra and Dobrovolny, 2019; Wethington et al., 2019; Beauchemin et al., 2019), none of these models have included the effect of syncytia. These studies all used ordinary differential equation (ODE) models, modeling viral infection of target cells and subsequent release of virus from infected cells. These models have been used to estimate RSV infection parameters (González-Parra and Dobrovolny, 2015, 2018a; González-Parra et al., 2018; Beauchemin et al., 2019), examine the role of the immune response (Wethington et al., 2019), and predict the effect of antiviral treatment (González-Parra and Dobrovolny, 2018b). The presence of syncytia could alter infection dynamics and affect the predictions of these models; particularly as it pertains to immune response and antiviral treatment as infection through syncytia formation allows the virus to avoid the extra-cellular space where components of the immune response and antivirals are active (Cifuentes-Munoz and Dutch, 2019).

The purpose of this study is to examine the role of syncytia on viral time course by examining the effect of model parameters such as the rate of virus production by syncytia and syncytia

* Corresponding author.
E-mail address: h.dobrovolny@tcu.edu (H.M. Dobrovolny).

https://doi.org/10.1016/j.jtbi.2021.110749
0022-5193/

lifespan. We will use computer simulations to model the viral titer to examine how viral titer time course changes as syncytia parameters are varied. We find that under some conditions, the involvement of syncytia in the infection can lead to long-lasting viral infections.

2. Material and methods

2.1. Mathematical model

We developed a new mathematical model of viral kinetics that includes the formation of syncytia. A schematic of the model is illustrated in Fig. 1. The virus, V, infects healthy target cells, T, at a rate β. The target cells become infected, I, and will produce more virus at rate p, or fuse with other cells to create syncytia, S, at rate γ. These syncytia cells then produce virus at a rate of $r_p p$. Both infected cells and syncytia continue to produce virus until they die after lifetimes of $1/\delta$ and $1/r_\delta\delta$ respectively. Virus is cleared from the system at a rate c. These processes are represented by the following equations,

$$\frac{dT}{dt} = -\beta TV - \gamma T(I+S) \frac{dI}{dt} = \beta TV - \gamma I(T+2I+S) - \delta I \frac{dS}{dt}$$
$$= \gamma T(2I+S) + \gamma I(2I+S) - r_\delta \delta S \frac{dV}{dt} = pI + r_p pS - cV. \quad (1)$$

Note that in these equations, S represents the number of cells that have fused into syncytia, not the number of syncytia. Thus when a target cell fuses with an infected cell, a cell is removed from each of the target and infected compartments and two cells appear in the syncytia compartment. We have a similar accounting when infected cells fuse to form syncytia — each syncytium consists of 2 infected cells. When a target cell or infected cell fuses with a cell already in a syncytium, we are only adding one new cell to the syncytia compartment.

Model parameters are taken from previous fits of viral kinetics models to data from RSV infections in African green monkeys (González-Parra and Dobrovolny, 2018b) and are given in Table 1. We use the median values determined from fits to Study 1 presented in Fig. 4 of that paper. Three parameters of this model have not been previously measured: syncytia fusion rate (γ), syncytia to cell death rate ratio (r_δ), and syncytia to cell production ratio (r_p). These parameters are varied over several orders of magnitude to explore their effect on viral dynamics.

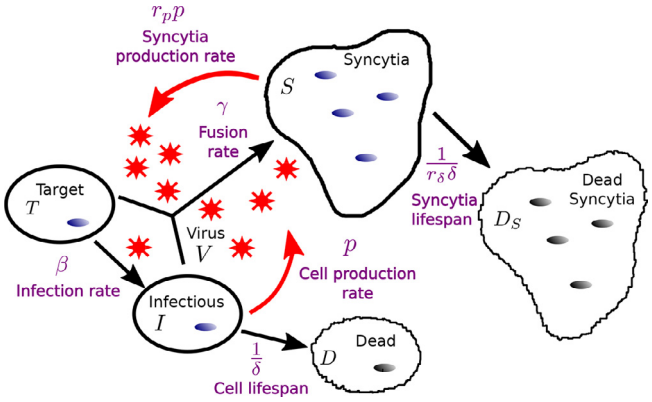

Fig. 1. Model of syncytia-inducing virus infection. The uninfected target cells can be infected by virus, or fused into syncytia. Infectious cells can be fused into syncytia or die. Both syncytia and infectious cells produce virus, although at different rates. Infectious cells and syncytia can also have different lifespans.

Table 1
Parameter values for simulation of RSV, taken from González-Parra and Dobrovolny (2018b).

Parameter	Value
Viral production rate (p)	4.66×10^6RNA/mL $\cdot$ h^{-1}
Infection rate (β)	2.04×10^{-8}(RNA/mL)$^{-1} \cdot$ h^{-1}
Clearance rate (c)	0.0763/h
Cell death rate (δ)	0.0735/h
Syncytia fusion rate (γ)	[0.01,1/h]
Syncytia to cell death rate ratio (r_δ)	$[1 \times 10^{-3}, 1 \times 10^3]$
Syncytia to cell viral production ratio (r_p)	$[1 \times 10^{-3}, 1 \times 10^3]$

2.2. Measurements

The model is simulated using the `odeint` function in the scipy package of python. We are interested in determining whether syncytia infectious lifespan and viral production rate alter the viral titer time course. We systematically vary r_p and r_δ and measure the following features of the viral load:

- **peak viral load:** The maximum amount of virus is commonly used as an indicator of the transmissibility of an infection (Handel et al., 2009).
- **time of viral peak:** This is the time between the start of the infection and the peak of the virus and can give an indication of how quickly the virus is replicating.
- **viral growth rate:** Viral upslope is the exponential growth rate of the viral titer before the peak is reached and is another indication of how quickly the virus is spreading from cell to cell.
- **viral decay rate:** Viral decay rate is the exponential decay rate of the viral titer after the peak. While the slope during the decay phase is negative, we define decay rate as the positive value of the slope.
- **area under the curve (AUC):** AUC is often used to assess the severity of an infection (Hayden et al., 2000; Barroso et al., 2005).
- **infection duration:** The infection duration is indicative of how long an infected patient might test positive for presence of the virus. We use a threshold of 10^4RNA/ML as in Dobrovolny et al. (2010).

We also use these measurements as endpoints for sensitivity analysis via partial rank correlation coefficients (PRCC). We sampled parameter values using Latin Hypercube Sampling within a range of $\pm$50% of their base value (Table 1) and used 1000 different parameter combinations to calculate the PRCC. The partial rank correlation coefficient is close to $\pm$1 if there is a high degree of correlation between the inputs (parameter values) and the outputs (measurements), with positive values indicating a positive correlation (both increase or decrease together) and negative values indicating a negative correlation.

3. Results

3.1. Role of syncytia fusion rate

Since this model is the first to include syncytia formation, appropriate values for the syncytia fusion rate are unknown. We first investigate model simulations with different values of syncytia fusion rate (γ) to determine what role it plays in the course of the infection. Fig. 2 shows the viral load (top left), fraction of target cells (top right), fraction of infectious mononucleated cells (bottom left), and fraction of cells in syncytia (bottom right) for several values of γ. As the syncytia fusion rate increases, the viral titer peak

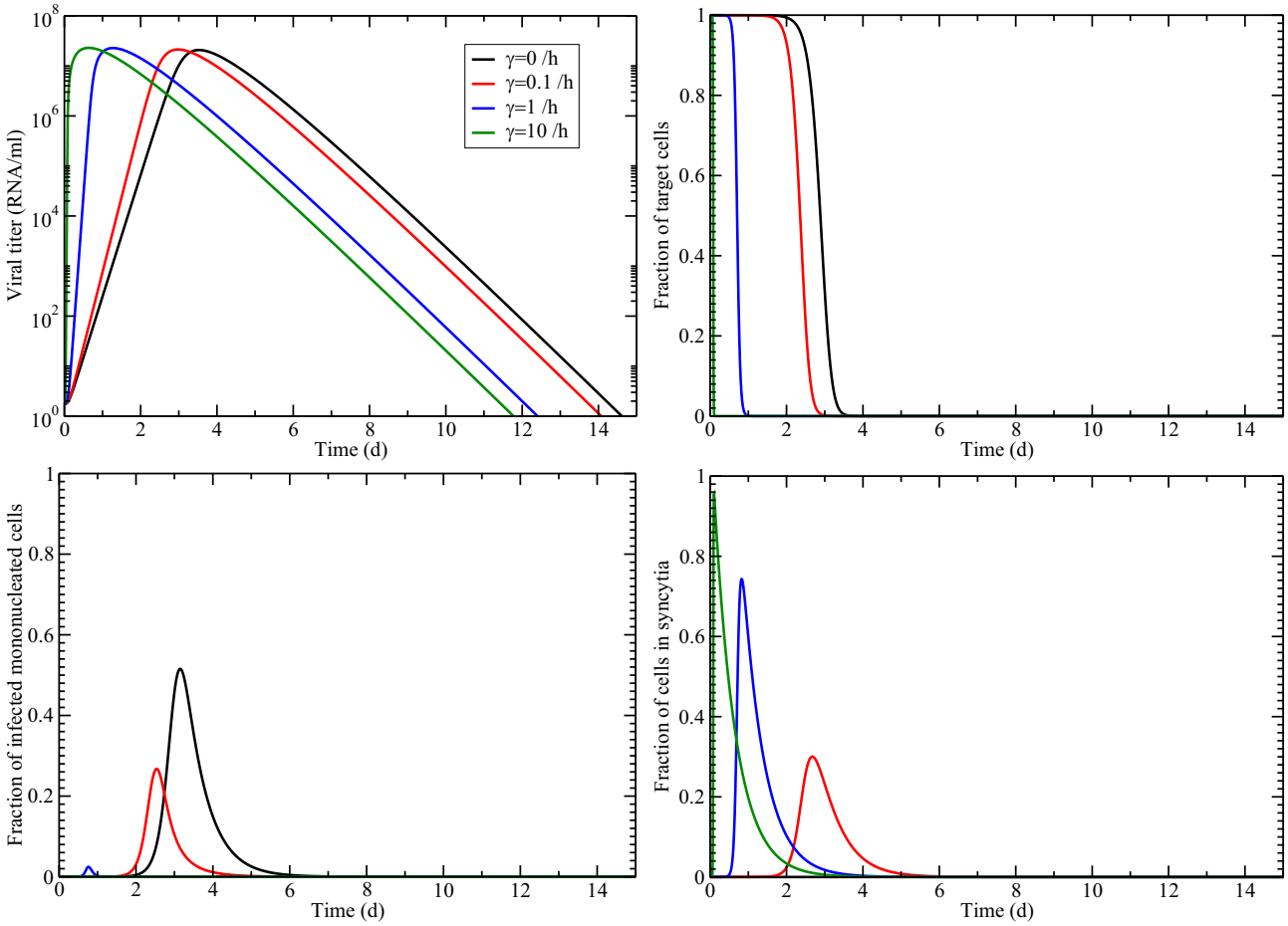

Fig. 2. The effect of syncytia fusion rate on time course of the infection. Figures show the viral load (top left), fraction of target cells (top right), fraction of infectious mononucleated cells (bottom left), and fraction of cells in syncytia (bottom right) for no syncytia formation (black line) and γ values of 0.1 (red lines), 1 (blue lines), and 10 (green lines). We assumed that cells in syncytia produced the same amount of virus and had the same lifespan as mononucleated cells ($r_\delta = r_p = 1$).

moves to the left (peaks earlier), but the viral load maintains the same viral peak. Target cells are also consumed faster as the syncytia fusion rate increases and the fraction of cells remaining mononucleated decreases as more cells are recruited into syncytia.

The changes in viral titer curves caused by changes in fusion rate are summarized in Fig. 3, which shows how our measured characteristics change with changes in fusion rate. When mononucleated cells have the same viral production rate and lifespan as cells in syncytia, some viral titer features (such as AUC, peak viral load and decay rate) are largely unaffected by changes in the fusion rate. We do, however, see a decrease in time of viral peak and infection duration, as well as an increase in viral growth rate as fusion rate increases. When we allow cells in syncytia and mononucleated cells to differ, either differing in viral production rate (red line) or cell death rate (green line), changes in fusion rate also change AUC, peak viral load and decay rate.

3.2. Viral titer changes caused by syncytia

Some of the broad behavior of the model is captured by the basic reproduction number, calculated via the next generation matrix method,

$$R_0 = \max\left(\frac{\gamma T_0}{r_\delta \delta}, \frac{\beta T_0 p}{c(\delta+\gamma T_0)} + \frac{\beta\gamma r_p p T_0^2}{c r_\delta \delta(\delta+\gamma T_0)}\right) = (R_f, R_{cf}+R_s).$$

The first term, R_f represents spread of the infection through fusion only. Note that when the infection is spreading through fusion only, it is not necessary to have any free virus. That is, we can have $R_f > 1$ and have no free virus. This means that this term does not determine when we see the effect of cell fusion on the viral time course. Whether or not there is growth of free virus is determined by the second term ($R_{cf}+R_s$), where the first part of this term represents the traditional infection route of virus released from one cell infecting other cells and the second part represents virus release from syncytia. The effect of syncytia becomes apparent in the viral load when the two pathways have similar reproduction numbers or

$$\frac{R_s}{R_{cf}} = \frac{\gamma r_p T_0}{r_\delta \delta} \approx 1. \tag{2}$$

This occurs for our parameters and $r_\delta = r_p = 1$ when $\gamma = 0.0735/\text{h}$.

The effect of syncytia parameters (γ, r_p, r_δ) on the virus-producing component of the basic reproduction number is shown in Fig. 4. When cells in syncytia are no different than other cells, the fusion rate does not change R_0. Once there is a difference in either viral production rate or lifespan, fusion rate either increases or decreases reaching a new asymptotic value of R_0 at high fusion rates. Large values of r_p and small values of r_δ lead to increasingly large values of R_0.

3.2.1. Rate of virus production by syncytia

We will fix the syncytia fusion rate to $\gamma = 0.1/\text{h}$ as this fusion rate ensures participation of syncytia without an unrealistically early viral titer peak. Fig. 5 shows the effect of relative rate of virus production by syncytia on viral titer time course (top) and viral

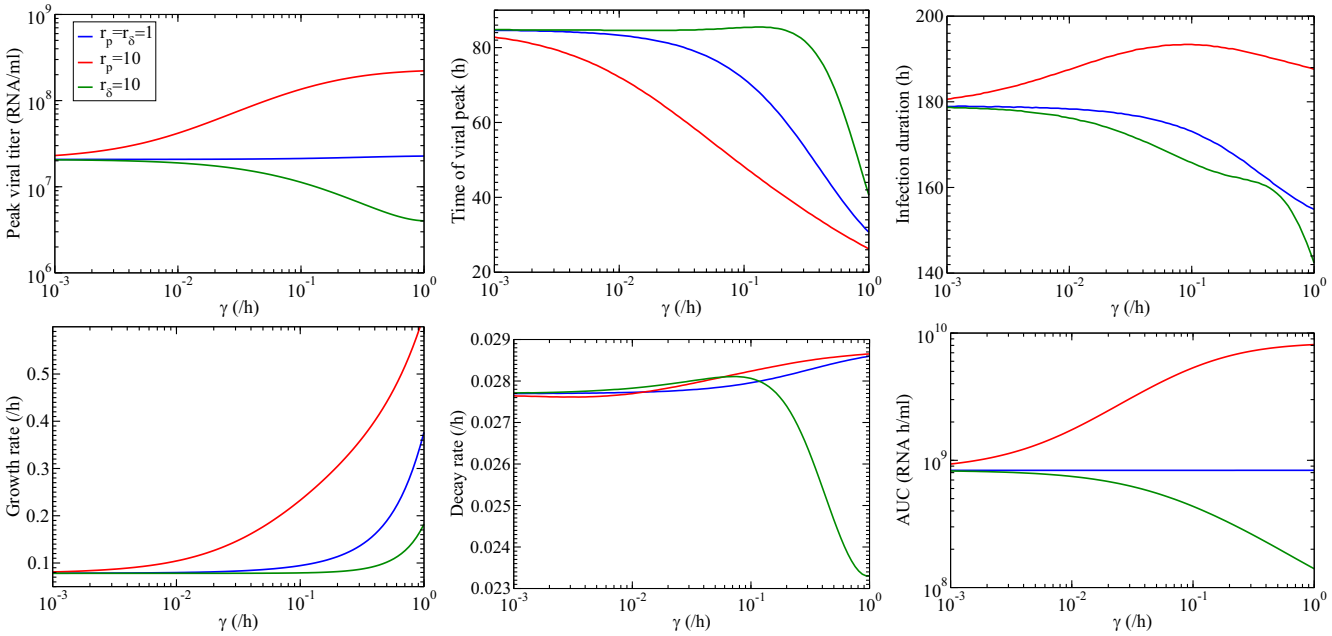

Fig. 3. The effect of syncytia fusion rate on characteristics of the viral titer time course. Top row shows the peak viral titer (left), time of viral titer peak (center), and infection duration as functions of syncytia fusion rate. Bottom row shows the growth rate (left), decay rate (center), and area under the viral curve (right) as functions of syncytia fusion rate. In all figures, the blue line shows the relationship when mononucleated cells and syncytia are identical; the red curve shows the relationship when syncytia have higher production ($r_p = 10$) and the green curve shows the relationship when syncytia have a shorter lifespan ($r_\delta = 10$).

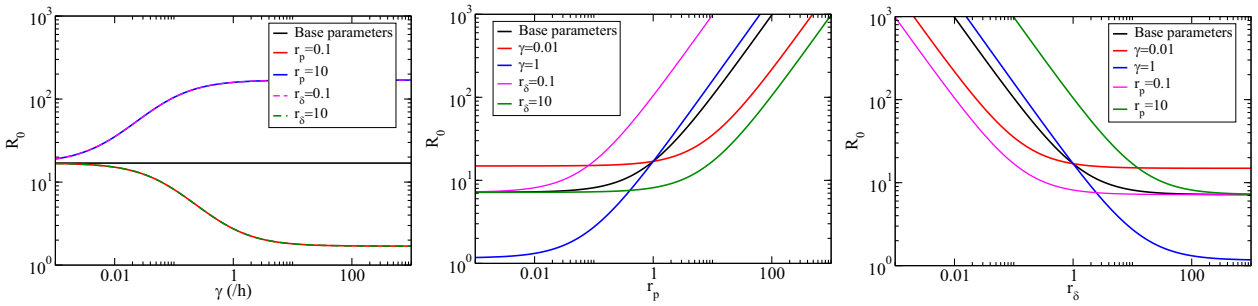

Fig. 4. The dependence of the virus-producing component of the basic reproduction number $R_0 = R_{cf} + R_s$ on syncytia parameters. Base parameters are $r_p = r_\delta = 1$ and $\gamma = 0.1$/h. Graphs show the dependence of R_0 on (left) γ, (center) r_p, and r_δ. In each graph, the remaining two parameters are varied by factors of 10 above and below the base parameters.

titer characteristics (center and bottom rows). Small values of r_p have little effect on the viral titer curve. For small r_p, the ratio R_s/R_{cf} is less than one and the presence of syncytia has little effect on viral time course. As we approach $R_s/R_{cf} = 1$ ($r_p = 0.735$, indicated by the vertical dashed line in the graphs), we start to see changes in the viral dynamics caused by increased syncytia viral production rate. When r_p becomes large ($r_p > 0.735$), the viral titer curve peaks earlier and at higher values. This is reflected in the viral titer characteristic measurements where we see peak viral load, infection duration, growth rate, and AUC all follow a similar trend of steadily increasing values for larger values of r_p. The two characteristics that show different trends are the decay rate, which remains essentially constant, and time of viral peak, which decreases for larger values of r_p.

3.2.2. Syncytia lifespan

Fig. 6 shows the effect of relative syncytia death rate on viral titer time course (top) and viral titer characteristics (center and bottom rows). Large values of r_δ correspond to small values of R_s/R_{cf} and the dashed line again indicates the r_δ value where $R_s/R_{cf} = 1$ ($r_\delta = 1.36$ for our parameters). When r_δ is large, syncytia lifespans are short so fewer cells get recruited into syncytia and mononucleated cells dominate at any given time during the infection since the syncytia disappear quickly. As the relative syncytia lifespan increases (r_δ decreases), the syncytia live long enough to produce some virus in the early phase of the infection increasing the growth rate and moving the time of peak earlier, but not yet affecting the decay rate of the viral curve. As the relative syncytia lifespan increases further, the syncytia start to outlive the mononucleated cells and we start to see a rapid decrease in the viral decay rate as the syncytia continue to produce virus over a long period of time. This also leads to a delay in the time of viral peak and increases in the infection duration and AUC.

The value of peak viral titer does not change much. Peak viral titer is given by $V_p = p(I_p + r_p S_p)/c$ (when $\frac{dV}{dt}$=0). This has a maximum possible value of p/c if all cells are infected or part of syncytia at the time of peak. At high values of r_δ, peak viral load is slightly reduced since cells that have fused into syncytia are dying off before the time of viral peak.

3.2.3. Slow growing infections

In the previous sections, we explored the effect of each syncytia variable by varying each separately from the others. This does not give a complete picture of the possible outcomes predicted by the

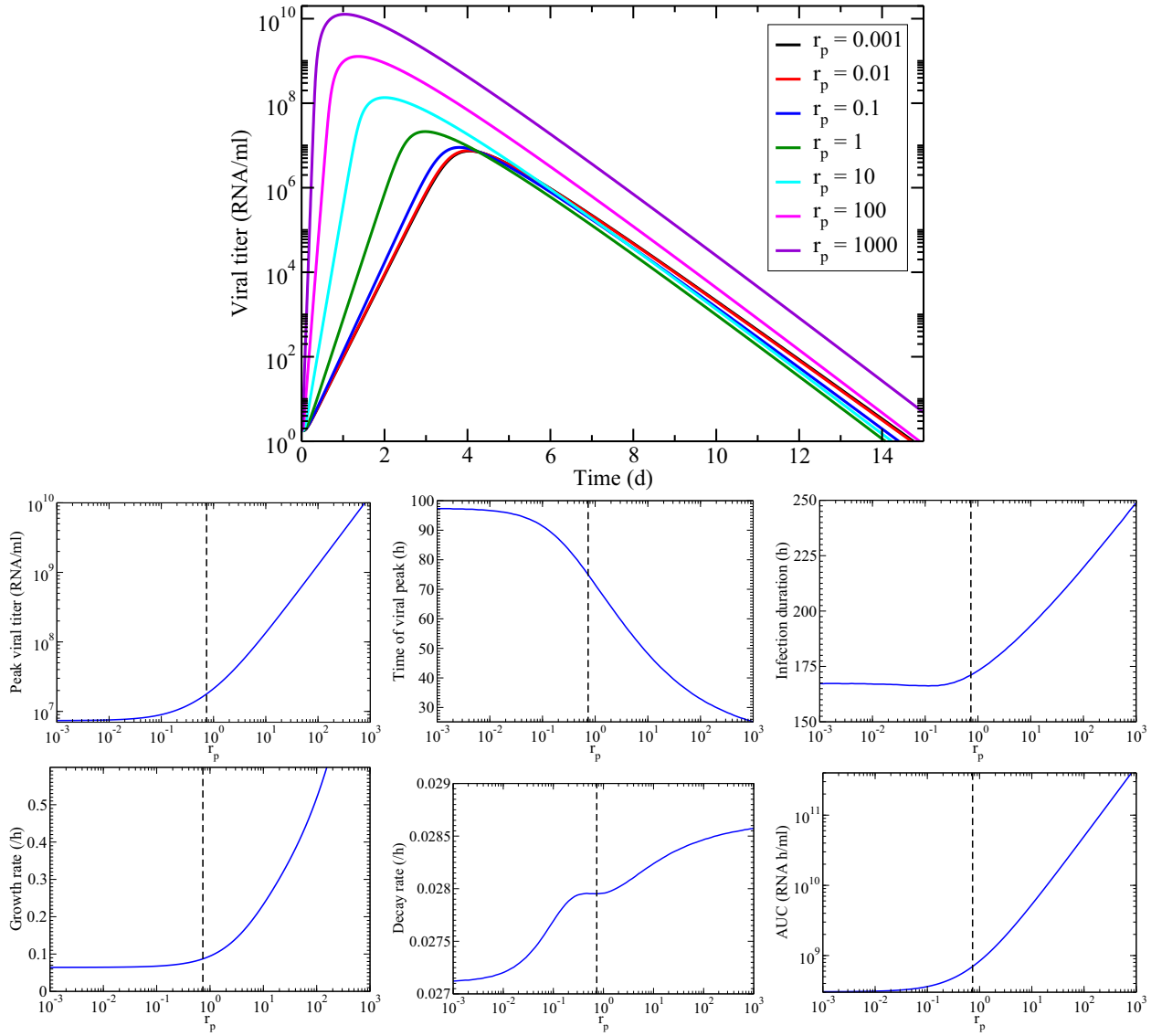

Fig. 5. The effect of relative rate of virus production by syncytia on time course of the infection. Top figure shows the viral titer for a range of relative rates of virus production by syncytia. Center row shows the peak viral titer (left), time of viral titer peak (center), and infection duration as functions of relative rate of virus production by syncytia. Bottom row shows the growth rate (left), decay rate (center), and area under the viral curve (right) as functions of relative rate of virus production by syncytia. Dashed vertical lines indicate the value of r_p where $R_s/R_{cf} = 1$.

model. Fig. 7 shows values of viral titer characteristics as both r_p and r_δ are varied. The left column shows predictions for a high syncytia fusion rate, the center column for an intermediate fusion rate (the same value of γ used in the previous two sections), and the right column shows a low value of syncytia fusion rate. For low syncytia fusion rate, there is little change in peak viral titer, time of viral peak, and viral growth rate.

At high fusion rate, there is a region with high syncytia death rate, but low viral production by syncytia that leads to long lasting infections. These infections are characterized by low viral growth rate and a delayed viral peak. The infection here is largely spread through syncytia formation and very little free virus is produced.

3.3. Sensitivity analysis

To further assess the role of all parameters in the course of the infection, we used partial rank correlation coefficient to determine the relative contribution of model parameters to infection characteristics (Fig. 8). The peak viral load is strongly correlated to viral production rates of both infected cells and syncytia, as would be expected, but also inversely correlated to death rates of infected cells and syncytia as well as viral clearance rate. The time of viral peak, however, is not strongly correlated to viral production. Instead, it is most strongly correlated to the cell death rates (both mononucleated infected cells and syncytia) as well as infection rate and viral clearance. The duration of the infection is most influenced by infection rate and viral clearance rate. The infection rate determines how quickly the viral load reaches the threshold of detection, while the viral clearance rate determines how quickly the virus drops below the threshold again. This is reflected in the PRCCs for growth rate, where β has the highest PRCC, and the PRCCs for decay rate, where c has the highest PRCC. The AUC is not strongly correlated with any one parameter, indicating that it contains information from all parts of the replication process.

4. Discussion

We explored a new ordinary differential equation model of viral infection that includes syncytia formation. The model suggests that syncytia formation will affect the viral titer time course when the

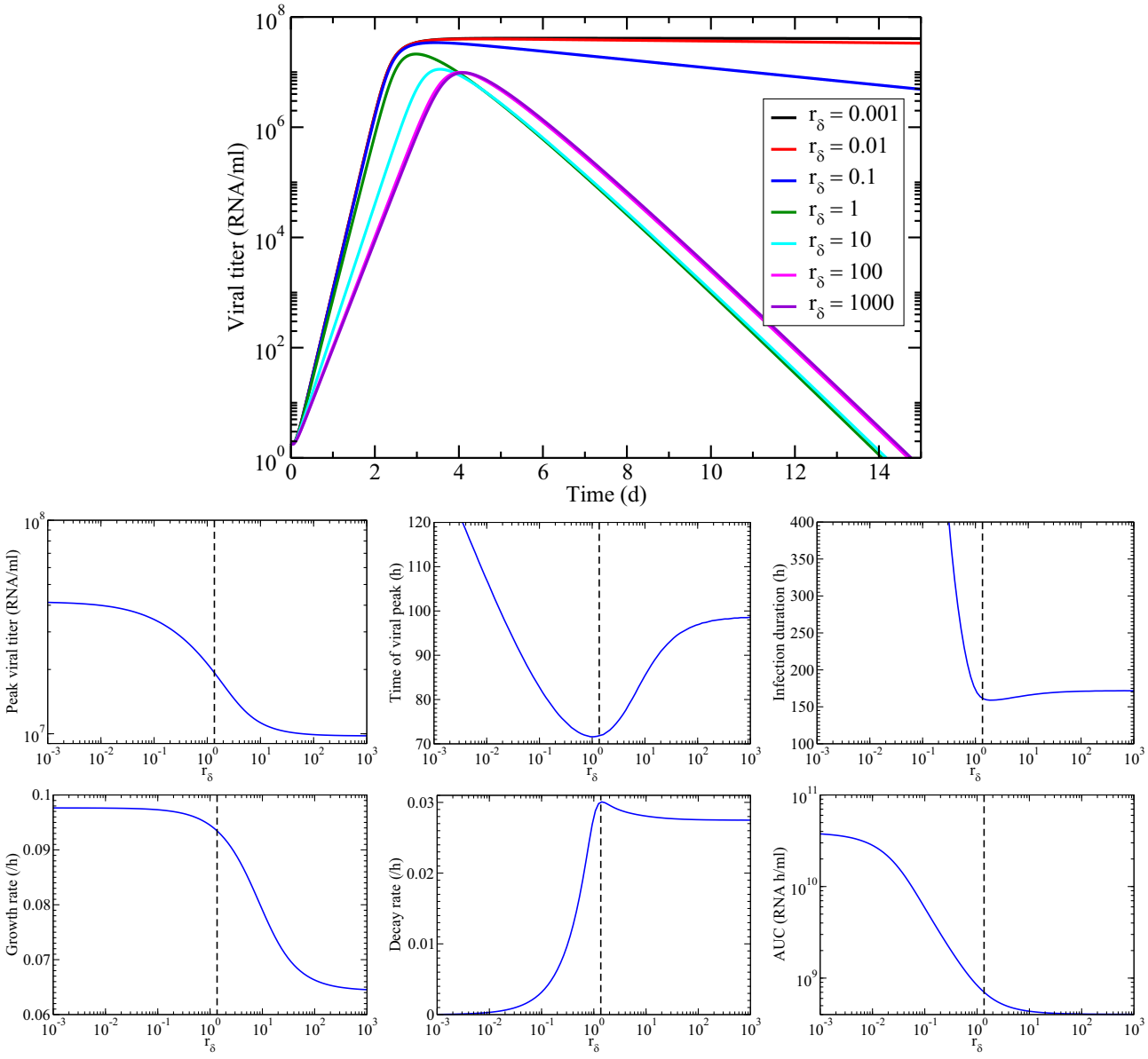

Fig. 6. The effect of relative syncytia death rate on time course of the infection. Top figure shows the viral titer for a range of relative syncytia death rates. Center row shows the peak viral titer (left), time of viral titer peak (center), and infection duration as functions of relative syncytia death rate. Bottom row shows the growth rate (left), decay rate (center), and area under the viral curve (right) as functions of relative syncytia death rate. Dashed vertical lines indicate the value of r_δ where $R_s/R_{cf} = 1$.

reproduction number for viral production from syncytia is similar to the reproduction number for viral production from mononuclear infected cells. Over most of the parameter space, the effect of syncytia is subtle, changing features of viral titer such as the peak viral load, time of peak, and growth rate. When the syncytia have long lifespans, we see long-lasting infections caused by continued viral production of long-lived syncytia. Another region of long-lasting infection is caused by slowly growing virus caused by a combination of suppressed production in syncytia and high syncytia formation rate. While RSV is typically an acute illness, there is evidence of long-lasting RSV infections in patients with hematological disorders (Lehners et al., 2016; Avetisyan et al., 2009) as well as immunocompromised ferrets (Stittelaar et al., 2016; de Waal et al., 2018). While a lack of immune response clearly plays a role in the persistence of these infections, it is not clear what role syncytia formation plays in the excessive duration of these infections. A recent in vitro study, however, indicates that persistent RSV infections in macrophages are caused by syncytia formation rather than by free virus (Ruiz-Gomez et al., 2021).

While our model shows a range of possible effects of the inclusion of syncytia, it is not clear the extent to which syncytia formation affects the time course of RSV since syncytia parameters such as syncytia fusion rate, rate of virus production by syncytia and syncytia lifespan have not been measured. Previous studies comparing RSV and influenza, a respiratory viral infection that does not cause syncytia formation, have noted that RSV has a slower growth rate and delayed time of viral peak as compared to influenza (Bagga et al., 2013; González-Parra et al., 2018). While other mechanisms, such as differences in virion diffusion, have been suggested as a reason for this difference, our study suggests that syncytia formation could be contributing to some of the observed dynamical differences.

Respiratory syncytial virus is not the only virus that can cause formation of syncytia. A number of other viruses have been shown to form syncytia including varicella-zoster virus (responsible for chicken pox and shingles) (Wang et al., 2017), rotavirus (Diller et al., 2019), human immunodeficiency virus (Symeonides et al., 2015), coronaviruses (responsible for Middle East respiratory syn-

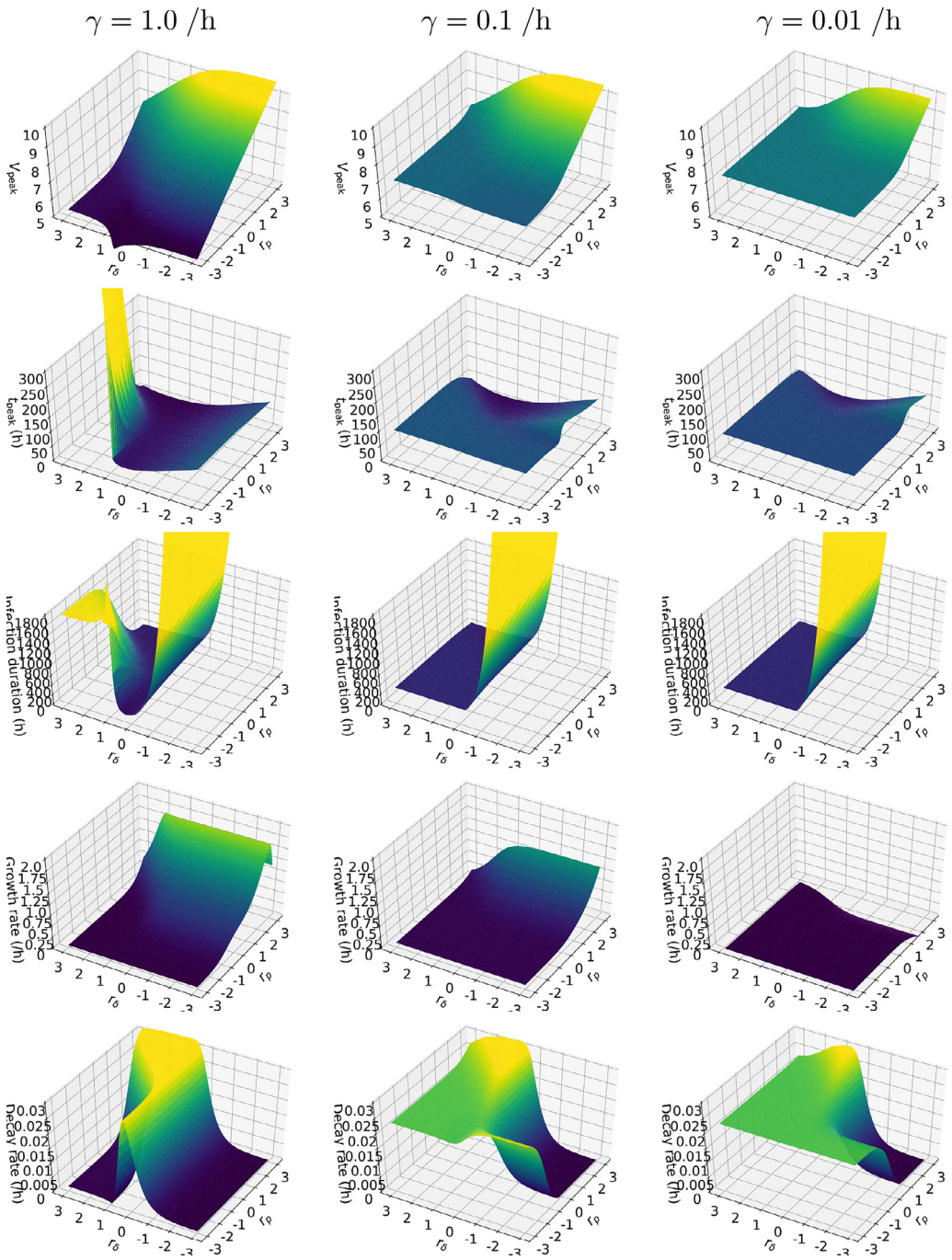

Fig. 7. Summary of viral titer characteristics. Each column shows the behavior of the model for different values of syncytia fusion rate: (left column) $\gamma = 1/\text{h}$, (center column) $\gamma = 0.1/\text{h}$, (right column) $\gamma = 0.01/\text{h}$. Each row shows one viral titer characteristic over a range of relative rates of virus production by syncytia and relative syncytia death rates: (top row) peak viral titer, (second row) time of viral peak, (third row) infection duration, (fourth row) viral growth rate, (fifth row) viral decay rate.

drome (MERS), severe acute respiratory syndrome (SARS), and coronavirus disease 2019 (COVID-19)) (Qian et al., 2013; Buchrieser et al., 2020), and measles (Ayata et al., 2007). The role of syncytia in the dynamics of these viruses has not been explored yet, so this model might also be able to provide some insight into the kinetics of these infections.

Validation and testing of the model via fitting to data will need to be done. Unfortunately, parameter identifiability is limited even for the standard viral kinetics models when only viral load data is used (Miao et al., 2011; Smith et al., 2010). This model adds a new pathway for continuation of the infection via syncytia formation that requires identification of additional parameters. In order to potentially identify these extra parameters, we need information on the time course of syncytia during an infection. While there are some experiments that have attempted to measure the number of syncytia and their size during in vitro RSV infections (Gagliardi et al., 2017; Van der Gucht et al., 2019) or during in vitro SARS-CoV-2 infections (Jacob et al., 2020), measurements are only made at one or two time points making it difficult to accurately estimate syncytia-related parameters.

This is a simplified model of the RSV replication cycle, and many features of RSV infections have been neglected. The immune response, for example, plays a role in RSV dynamics (Efstathiou et al., xxxx; Glaser et al., 2019; Bhat et al., 2020), but was neglected in this model. It has been suggested that syncytia formation might be a mechanism for viral immune evasion (Cifuentes-Munoz and

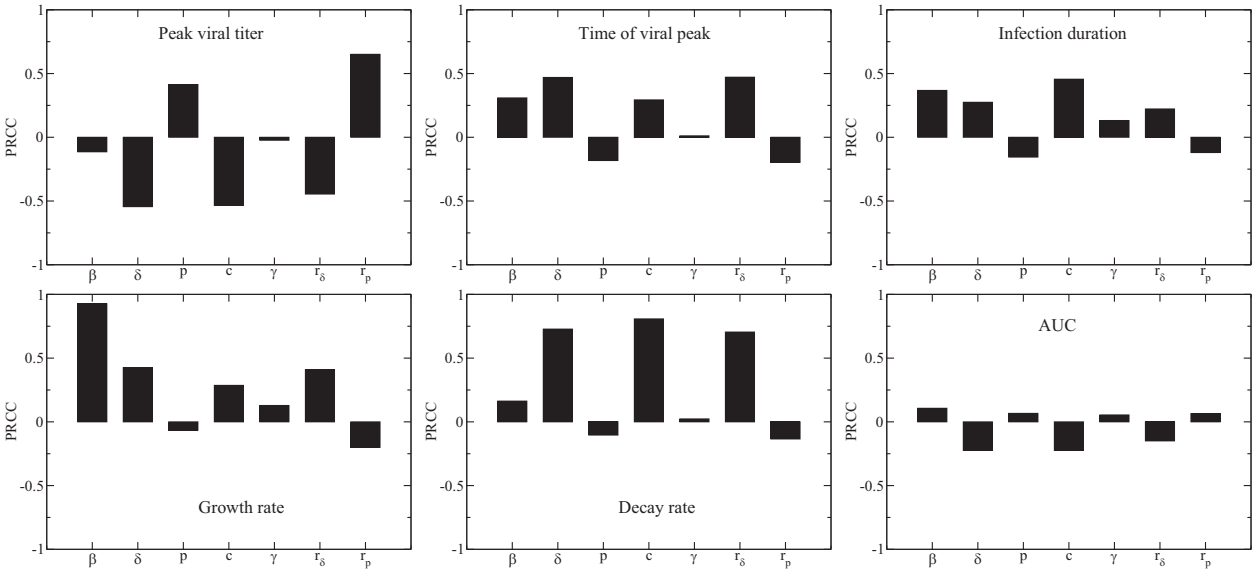

Fig. 8. Sensitivity analysis using partial rank correlation coefficients. Figures show the partial rank correlation coefficients for parameter correlations with peak viral load (top left), time of viral peak (top center), infection duration (top right), viral growth rate (bottom left), viral decay rate (bottom center), and AUC (bottom left).

Dutch, 2019), so there is possible interplay between syncytia formation and the immune response that could alter viral time course. We have also not included an eclipse phase in our model to account for delay in viral production after cells have been infected (Baccam et al., 2006). The inclusion of an eclipse phase is not straightforward here since it isn't clear if newly fused target cells should have an eclipse phase or a modified eclipse phase. It is also likely that the eclipse phase for viral production differs from the time at which an infected cell can start to initiate fusion since the first requires all components of the virus to be produced, migrate to the surface, and get released, while the second can occur as soon as surface proteins are produced and migrate to the cell surface (Martinez and Melero, 2000; Feldman et al., 2000). While the lack of an eclipse phase should not change the general trends we observe, the incorporation of an eclipse phase would result in a later and more biologically accurate time of peak (González-Parra et al., 2018; González-Parra and Dobrovolny, 2018a). We further assumed exponential transitions for death of both mononucleated cells as well as syncytia. There is evidence from other viruses that the exponential assumption for cell death is not biologically accurate (Beauchemin et al., 2017) for mononucleated cells. It is most certainly not accurate for syncytia since all the cells in a syncytium will die at once, so a bursting model (Chen et al., 2007; Perelson et al., 1996) might be more appropriate for syncytia death. Finally, our use of an ordinary differential equation model neglects the spatial dynamics that are inherent in the formation of syncytia (Alzahrani et al., 2020; Jacobsen and Pilyugin, 2015).

Although there are limitations in our mathematical model, we nonetheless gained insight into the role played by syncytia in the course of the infection. In particular, our model indicates that the formation of syncytia does not manifest itself in viral load dynamics until the viral production by syncytia formation is similar in scale to viral production via spread of cell-free virus.

CRediT authorship contribution statement

Benjamin Jessie: Software, Formal analysis, Writing - original draft, Writing - review & editing. **Hana M. Dobrovolny:** Conceptualization, Methodology, Validation, Writing - review & editing, Supervision, Project administration.

Declaration of Competing Interest

The authors declare that they have no known competing financial interests or personal relationships that could have appeared to influence the work reported in this paper.

Acknowledgements

Thank you to the anonymous reviewers whose helpful suggestions improved the manuscript. This work was supported by a grant from Texas Christian University's Research and Creative Activities Fund.

References

Ali, A., Lopardo, G., Scarpellini, B., Stein, R.T., Ribeiro, D., 2020. Systematic review on respiratory syncytial virus epidemiology in adults and the elderly in Latin America. Intl. J. Infect. Dis. 170, 170–180. https://doi.org/10.1016/j.ijid.2019.10.025.

Alzahrani, T., Eftimie, R., Trucu, D., 2020. Multiscale moving boundary modelling of cancer interactions with a fusogenic oncolytic virus: The impact of syncytia dynamics. Math. Biosci. 323, 108296.

Avetisyan, G., Mattsson, J., Sparrelid, E., Ljungman, P., 2009. Respiratory syncytial virus infection in recipients of allogeneic stem-cell transplantation: A retrospective study of the incidence, clinical features, and outcome. Transplant. 88 (10), 1222–1226. https://doi.org/10.1097/TP.0b013e3181bb477e.

Ayala-Breton, C., Russell, L.O., Russell, S.J., Peng, K.-W., 2014. Faster replication and higher expression levels of viral glycoproteins give the vesicular stomatitis virus/measles virus hybrid vsv-fh a growth advantage over measles virus. J. Virol. 88 (15), 8332–8339. https://doi.org/10.1128/JVI.03823-13.

Ayata, M., Shingai, M., Ning, X., Matsumoto, M., Seya, T., Otani, S., Seto, T., Ohgimoto, S., Ogura, H., 2007. Effect of the alterations in the fusion protein of measles virus isolated from brains of patients with subacute sclerosing panencephalitis on syncytium formation. Virol. Res. 130 (1–2), 260–268. https://doi.org/10.1016/j.vir-usres.2007.07.017.

Baccam, P., Beauchemin, C., Macken, C.A., Hayden, F.G., Perelson, A.S., 2006. Kinetics of influenza A virus infection in humans. J. Virol. 80 (15), 7590–7599. https://doi.org/10.1128/JVI.01623-05.

Bagga, B., Woods, C.W., Veldman, T.H., Gilbert, A., Mann, A., Balaratnam, G., Lambkin-Williams, R., Oxford, J.S., McClain, M.T., Wilkinson, T., Nicholson, B.P., Ginsburg, G. S., DeVincenzo, J.P., 2013. Comparing influenza and RSV viral disease dynamics in experimentally infected adults predicts clinical effectiveness of RSV antivirals. Antivir. Ther. 18, 785–791. https://doi.org/10.3851/IMP2629.

Barroso, L., Treanor, J., Gubareva, L., Hayden, F.G., 2005. Efficacy and tolerability of the oral neuraminidase inhibitor peramivir in experimental human influenza: randomized, controlled trials for prophylaxis and treatment. Antivir. Ther. 10, 901–910.

Beauchemin, C.A., Miura, T., Iwami, S., 2017. Duration of SHIV production by infected cells is not exponentially distributed: Implications for estimates of infection parameters and antiviral efficacy. Sci. Rep. 7, 42765. https://doi.org/10.1038/srep42765.

Beauchemin, C.A., Kim, Y.-I., Yu, Q., Ciaramella, G., DeVincenzo, J.P., 2019. Uncovering critical properties of the human respiratory syncytial virus by combining in vitro assays and in silico analyses. Plos One 14, (4). https://doi.org/10.1371/journal.pone.0214708 e0214708.

Bem, R.A., Domachowske, J.B., Rosenberg, H.F., 2011. Animal models of human respiratory syncytial virus disease. Am. J. Physiol. 301 (2), L148–L156. https://doi.org/10.1152/ajplung.00065.2011.

Bhat, R., Farrag, M.A., Almajhdi, F.N., 2020. Double-edged role of natural killer cells during RSV infection. Intl. Rev. Immunol. 39 (5), 233–244. https://doi.org/10.1080/08830185.2020.1770748.

Buchrieser, J., Dufloo, J., Hubert, M., Monel, B., Planas, D., Rajah, M.M., Planchais, C., Porrot, F., Guivel-Benhassine, F., der Werf, S.V., Casartelli, N., Mouquet, H., Bruel, T., Schwartz, O., 2020. Syncytia formation by sars-cov-2 infected cells, BioRxiv doi:10.1101/2020.07.14.202028..

Chen, H.Y., Di Mascio, M., Perelson, A.S., Ho, D.D., Zhang, L., 2007. Determination of virus burst size in vivo using a single-cycle SIV in rhesus macaques. Proc. Natl. Acad. Sci. U.S.A. 104 (48), 19079–19084. https://doi.org/10.1073/pnas.0707449104.

Cifuentes-Munoz, N., Dutch, R.E., 2019. To assemble or not to assemble: The changing rules of pneumovirus transmission. Virus Res. 265, 68–73. https://doi.org/10.1016/j.virusres.2019.03.002.

de Waal, L., Smits, S.L., Kroeze, E.J.V., van Amerongen, G., Pohl, M.O., Osterhaus, A.D., Stittelaar, K.J., 2018. Transmission of human respiratory syncytial virus in the immunocompromised ferret model. Viruses 10 (1), 18. https://doi.org/10.3390/v10010018.

Diller, J.R., Parrington, H.M., Patton, J.T., Ogden, K.M., 2019. Rotavirus species B encodes a functional fusion-associated small transmembrane protein. J. Virol. 93 (20), e00813–19. https://doi.org/10.1128/JVI.00813-19.

Dobrovolny, H.M., Baron, M.J., Gieschke, R., Davies, B.E., Jumbe, N.L., Beauchemin, C. A.A., 2010. Exploring cell tropism as a possible contributor to influenza infection severity. PLoS ONE 5, (11). https://doi.org/10.1371/journal.pone.0013811 e13811.

Domachowske, J., Bonville, C., Rosenberg, H., 2000. Cytokeratin 17 is expressed in cells infected with respiratory syncytial virus via NF-kappa B activation and is associated with the formation of cytopathic syncytia. J. Infect. Dis. 182 (4), 1022–1028. https://doi.org/10.1086/315841.

Drews, S.J., Branche, A.R., Falsey, A.R., Lee, N., 2019. What is the role of rapid molecular testing for seniors and other at-risk adults with respiratory syncytial virus infections?. J. Clin. Virol. 117, 27–32. https://doi.org/10.1016/j.jcv.2019.05.010.

Efstathiou, C., Abidi, S., Harker, J., Stevenson, N. Revisiting respiratory syncytial virus's interaction with host immunity, towards novel therapeutics, Cell. Mol. Life Sci. doi:10.1007/s00018-020-03557-0..

Feldman, S., Audet, S., Beeler, J., 2000. The fusion glycoprotein of human respiratory syncytial virus facilitates virus attachment and infectivity via an interaction with cellular heparan sulfate. J. Virol. 74 (14), 6442–6447. https://doi.org/10.1128/JVI.74.14.6442-6447.2000.

Gagliardi, T.B., Criado, M.F., Proenca-Modena, J.L., Saranzo, A.M., Iwamoto, M.A., de Paula, F.E., Cardoso, R.S., Delcaro, L.S., Silva, M.L., Camara, A.A., Arruda, E., 2017. Syncytia induction by clinical isolates of human respiratory syncytial virus A. Intervirol. 60 (1–2), 56–60. https://doi.org/10.1159/000480014.

Glaser, L., Coulter, P., Shields, M., Touzelet, O., Power, U.F., Broadbent, L., 2019. Airway epithelial derived cytokines and chemokines and their role in the immune response to respiratory syncytial virus infection. Pathogens 8 (3), 106. https://doi.org/10.3390/pathogens8030106.

González-Parra, G., Dobrovolny, H.M., 2015. Assessing uncertainty in A2 respiratory syncytial virus viral dynamics. Comput. Math. Meth. Med. 2015,. https://doi.org/10.1155/2015/567589 567589.

González-Parra, G., Dobrovolny, H.M., 2018a. A quantitative assessment of dynamical differences of RSV infections in vitro and in vivo. Virol. 523, 129–139. https://doi.org/10.1016/j.virol.2018.07.027.

González-Parra, G., Dobrovolny, H.M., 2018b. Modeling of fusion inhibitor treatment of RSV in African green monkeys. J. Theor. Biol. 456, 62–73. https://doi.org/10.1016/j.jtbi.2018.07.029.

González-Parra, G., Dobrovolny, H.M., 2019. The rate of viral transfer between upper and lower respiratory tracts determines RSV illness duration. J. Math. Biol. 79, 467–483. https://doi.org/10.1007/s00285-019-01364-1.

González-Parra, G., De Ridder, F., Huntjens, D., Roymans, D., Ispas, G., Dobrovolny, H. M., 2018. A comparison of RSV and influenza in vitro kinetic parameters reveals differences in infecting time. Plos One 13, (2). https://doi.org/10.1371/journal.pone.0192645 e0192645.

Gonzalez-Reyes, L., Ruiz-Arguello, M., Garcia-Barreno, B., Calder, L., Lopez, J., Albar, J., Skehel, J., Wiley, D., Melero, J., 2001. Cleavage of the human respiratory syncytial virus fusion protein at two distinct sites is required for activation of membrane fusion. Proc. Natl. Acad. Sci. U.S.A. 98 (17), 9859–9864. https://doi.org/10.1073/pnas.151098198.

Handel, A., Longini, I.M., Antia, R., 2009. Antiviral resistance and the control of pandemic influenza: The roles of stochasticity, evolution and model details. J Theor. Biol. 256, 117–125. https://doi.org/10.1016/j.jtbi.2008.09.021.

Hayden, F., Jennings, L., Robson, R., Schiff, G., Jackson, H., Rana, B., McClelland, G., Ipe, D., Roberts, N., Ward, P., 2000. Oral oseltamivir in human experimental influenza b infection. Antivir. Ther. 5 (3), 205–213.

Hu, M., Bogoyevitch, M.A., Jans, D.A., 2020. Impact of respiratory syncytial virus on host functions: Implications for antiviral strategies. Physiol. Rev. 100 (4), 1527–1594. https://doi.org/10.1152/physrev.00030.2019.

Jacob, F., Pather, S.R., Huang, W.-K., Zhang, F., Wong, S.Z.H., Zhou, H., Cubitt, B., Fan, W., Chen, C.Z., Xu, M., Pradhan, M., Zhang, D.Y., Zheng, W., Bang, A.G., Song, H., de la Torre, J.C., li Ming, G., 2020. Human pluripotent stem cell-derived neural cells and brain organoids reveal SARS-CoV-2 neurotropism predominates in choroid plexus epithelium. Cell Stem Cell 27 (6), 937–951. doi:10.1016/j.stem.2020.09.016..

Jacobsen, K., Pilyugin, S.S., 2015. Analysis of a mathematical model for tumor therapy with a fusogenic oncolytic virus. Math. Biosci. 270, 169–182. https://doi.org/10.1016/j.mbs.2015.02.009.

Lehners, N., Tabatabai, J., Prifert, C., Wedde, M., Puthenparambil, J., Weissbrich, B., Biere, B., Schweiger, B., Egerer, G., Schnitzler, P., 2016. Long-term shedding of influenza virus, parainfluenza virus, respiratory syncytial virus and nosocomial epidemiology in patients with hematological disorders. PLoS ONE 11, (2). https://doi.org/10.1371/journal.pone.0148258 e0148258.

Martinez, I., Melero, J., 2000. Binding of human respiratory syncytial virus to cells: implication of sulfated cell surface proteoglycans. J. Gen. Virol. 81, 2715–2722. https://doi.org/10.1099/0022-1317-81-11-2715.

Miao, H., Xia, X., Perelson, A.S., Wu, H., 2011. On identifiability of nonlinear ODE models and applications in viral dynamics. SIAM Rev. 53 (1), 3–39. https://doi.org/10.1137/090757009.

Perelson, A.S., Neumann, A., Markowitz, M., Leonard, J., Ho, D., 1996. HIV-1 dynamics in vivo: Virion clearance rate, infected cell life-span, and viral generation time. Science 271 (5255), 1582–1586.

Piva, H.M., Sa, J.M., Miranda, A.S., Tasic, L., Fossey, M.A., Souza, F.P., Caruso, I.P., 2020. Insights into interactions of flavanones with target human respiratory syncytial virus M2–1 protein from STD-NMR, fluorescence spectroscopy, and computational simulations. Intl. J. Mol. Sci. 21 (6), 2241. https://doi.org/10.3390/ijms21062241.

Porotto, M., Ferren, M., Chen, Y.-W., Siu, Y., Makhsous, N., Rima, B., Briese, T., Greninger, A., Snoeck, H.-W., Moscona, A., 2019. Authentic modeling of human respiratory virus infection in human pluripotent stem cell-derived lung organoids. MBIO 10 (3), e00723–19. https://doi.org/10.1128/mBio.00723-19.

Qian, Z., Dominguez, S.R., Holmes, K.V., 2013. Role of the spike glycoprotein of human middle east respiratory syndrome coronavirus (MERS-CoV) in virus entry and syncytia formation. PLoS ONE 8, (10). https://doi.org/10.1371/journal.pone.0076469 e76469.

Ruiz-Gomez, X., Vazquez-Perez, J.A., Flores-Herrera, O., Esparza-Perusqua, M., Santiago-Olivares, C., Gaona, J., Gomez, B., Mejia-Nepomuceno, F., Mendez, C., Rivera-Toledo, E., 2021. Steady-state persistence of respiratory syncytial virus in a macrophage-like cell line and sequence analysis of the persistent viral genome. Virus Res. https://doi.org/10.1016/j.virusres.2021.198367 198367.

Saleh, F., Harb, A., Soudani, N., Zaraket, H., 2020. A three-dimensional A549 cell culture model to study respiratory syncytial virus infections. J. Infect. Pub. Health 13 (8), 1142–1147. https://doi.org/10.1016/j.jiph.2020.03.011.

Smith, A.M., Adler, F.R., Perelson, A.S., 2010. An accurate two-phase approximate solution to an acute viral infection model. J. Math. Biol. 60 (5), 711–726. https://doi.org/10.1007/s00285-009-0281-8.

Stittelaar, K.J., de Waal, L., van Amerongen, G., Kroeze, E.J.V., Fraaij, P.L., van Baalen, C.A., van Kampen, J.J., van der Vries, E., Osterhaus, A.D., de Swart, R.L., 2016. Ferrets as a novel animal model for studying human respiratory syncytial virus infections in immunocompetent and immunocompromised hosts. Viruses 8 (6), 168. https://doi.org/10.3390/v8060168.

Symeonides, M., Murooka, T.T., Bellfy, L.N., Roy, N.H., Mempel, T.R., Thali, M., 2015. HIV-1-induced small T cell syncytia can transfer virus particles to target cells through transient contacts. Viruses 7 (12), 6590–6603. https://doi.org/10.3390/v7122959.

Taylor, G., 2017. Animal models of respiratory syncytial virus infection. Vaccine 35 (3), 469–480. https://doi.org/10.1016/j.vaccine.2016.11.054.

Tin Tin Htar, M., Yerramalla, M., Moisi, J., Swerdlow, D., 2020. The burden of respiratory syncytial virus in adults: a systematic review and meta-analysis, Epidemiol. Infect. 148, e48. doi:10.1017/S0950268820000400..

Toivonen, L., Karppinen, S., Schuez-Havupalo, L., Teros-Jaakkola, T., Mertsola, J., Waris, M., Peltola, V., 2020. Respiratory syncytial virus infections in children 0–24 months of age in the community. J. Infect. 80 (1), 69–75. https://doi.org/10.1016/j.jinf.2019.09.002.

Van der Gucht, W., Stobbelaar, K., Govaerts, M., Mangodt, T., Barbezange, C., Leemans, A., De Winter, B., Van Gucht, S., Caljon, G., Maes, L., De Dooy, J., Jorens, P., Smet, A., Cos, P., Verhulst, S., Delputte, P.L., 2019. Isolation and characterization of clinical RSV isolates in Belgium during the winters of 2016–2018. Viruses 11 (11), 1031. https://doi.org/10.3390/v11111031.

Walsh, E.E., Peterson, D.R., Kalkanoglu, A.E., Lee, F.E.-H., Falsey, A.R., 2004. Risk factors for severe respiratory syncytial virus infection in elderly persons. J. Infect. Dis. 189, 233–238.

Walsh, E.E., Peterson, D.R., Falsey, A.R., 2013. Viral shedding and immune responses to respiratory syncytial virus infection in older adults. J. Infect. Dis. 207, 1424–1432. https://doi.org/10.1093/infdis/jit038.

Wang, W., Yang, L., Huang, X., Fu, W., Pan, D., Cai, L., Ye, J., Liu, J., Xia, N., Cheng, T., Zhu, H., 2017. Outer nuclear membrane fusion of adjacent nuclei in varicella-zoster virus-induced syncytia. Virol. 512, 34–38. https://doi.org/10.1016/j.virol.2017.09.002.

Wethington, D., Harder, O., Uppulury, K., Stewart, W.C., Chen, P., King, T., Reynolds, S.D., Perelson, A.S., Peeples, M.E., Niewiesk, S., Das, J., 2019. Mathematical modelling identifies the role of adaptive immunity as a key controller of respiratory syncytial virus in cotton rats. J. Roy. Soc. Interface 16 (160), 20190389. https://doi.org/10.1098/rsif.2019.0389.